Metal Oxide−Support Interactions in Fe/ZrO_2 Catalysts

Yasuaki Okamoto,*,† Takeshi Kubota,† Yoshiharu Ohto,‡ and Saburo Nasu§

Department of Material Science, Shimane University, Matsue 690-8504, Japan, Department of Chemical Engineering, Faculty of Engineering Science, Osaka University, Toyonaka, Osaka 560-8531, Japan, and Department of Physical Science, Graduate School of Engineering Science, Osaka University, Toyonaka, Osaka 560-8531, Japan

Received: November 18, 1999; In Final Form: May 25, 2000

To reveal the metal oxide−support interactions in ZrO_2-supported Fe oxide catalysts as a function of calcination temperature, 5 wt % Fe/ZrO_2 was characterized by means of ^{57}Fe Mössbauer spectroscopy, IR, XRD, and thermogravimetric analysis. The catalytic activity of Fe/ZrO_2 was examined at 523 K for NO−CO reaction. It is shown that when Fe/ZrO_2 is calcined below 573 K, small particles of hydrated Fe^{3+} oxyhydroxides (superparamagnetic at 297 K) are formed together with Fe^{3+} paramagnetic species ion-exchanged with the surface OH groups of ZrO_2. In addition to the Fe^{3+} ion-exchanged species, Fe^{3+} oxide clusters and crystalline α-Fe_2O_3 particles are formed by successive dehydration of the oxyhydroxides on calcination at 973 K. When Fe/ZrO_2 is calcined at 1073 or 1173 K, the Mössbauer spectroscopic results suggest the formation of Fe^{3+} cations trapped in surface vacant sites of ZrO_2 at the expense of the Fe^{3+} oxide clusters. On the calcination at a higher temperature, crystalline α-Fe_2O_3 predominates with a small portion of the Fe^{3+} cations being in surface vacant sites. With 2 wt % Fe/ZrO_2 prepared by a coprecipitation method and calcined at 1173−1373 K, Fe^{3+} cations dissolved in a ZrO_2 lattice are formed in addition to a small amount of magnetically split component.

Introduction

Understanding of metal oxide−support interactions in supported metal oxide catalysts is one of the most important subjects for the research in catalysis, since their performance is greatly affected by the support material, loading level, catalyst precursor, calcination temperature, and so on. Extensive studies[1−10] have been carried out to reveal the nature of the interaction species for a variety of metal oxide catalysts, in particular supported on Al_2O_3 or SiO_2, because of their industrial importance. Several interaction modes are claimed to be present, depending on the preparation variables. The interaction modes include subsurface species, cationic species trapped in surface vacant sites, isolated surface species, monolayer oxide species, metal oxide clusters, as well as small metal oxide crystalline or amorphous particles.

Recently, ZrO_2 has received increasing attention as catalysts and catalyst support.[11] ZrO_2-supported Cr,[12] Cu,[13−16] and Fe[13,17] oxides have been shown to be highly active for NO reduction by CO and oxidation of CO at a low temperature. The catalytic behavior of Fe oxides supported on ZrO_2 has also been studied by Boot[18] for the dehydrogenation of butene. Perovskite-type mixed oxides,[19,20] $LaCoO_3$, and La_2CuO_4, supported on ZrO_2, have been reported to be very active for propane oxidation and NO−CO reaction. Furthermore, the activity of a SO_4/ZrO_2 solid superacid catalyst is greatly improved by the addition of Fe and Mn oxides.[21−24] Despite high feasibility of ZrO_2-supported metal oxide catalysts for NO−CO and CO oxidation reactions, the knowledge of the interaction modes between metal oxide and the surface of ZrO_2 is considerably limited.

With Cu/ZrO_2,[15] it has been shown using EXAFS that highly dispersed Cu^{2+} species in an octahedral symmetry predominate at a Cu content lower than 1 wt %. Copper oxide clusters are formed upon an additional loading of Cu. An IR study[15] of surface OH groups has shown that highly dispersed Cu^{2+} species are produced by preferential reactions with terminal OH groups of the ZrO_2 surface. UV−vis near-infrared spectra of Cu/ZrO_2 dried at 383 K suggest ion-exchange of the OH groups with Cu^{2+} cations in aqueous ammonia solution.[25] It is claimed by temperature-programmed reduction of Cu/ZrO_2 using CO as a reducing gas that the dispersion and stability of Cu_2O are improved by the interaction with the ZrO_2 surface.[26] ZrO_2-supported Cr oxide has been studied by Yamaguchi et al.[12] by means of XRD and ESR. Two-dimensional octahedral or square pyramidal Cr oxide species are suggested to form on the ZrO_2 surface at a low Cr content. It is revealed[27] that when La−Co/ZrO_2 is calcined at 1123 K, $LaCoO_3$ perovskite is formed in a highly dispersed state as fine particles or thin overlayers on the surface of ZrO_2 below the loading level of 5 wt %. However, the nature of the metal oxide−support interactions has not been explored in sufficient detail yet.

In our previous work,[13,17] it has been found that Fe/ZrO_2 exhibits a very high activity for the reduction of NO by CO above 500 K. With Fe oxides supported on ZrO_2, the formation of well-dispersed Fe^{3+} oxides is suggested by Ji et al.[28] using XAFS at a very low loading of Fe (0.5 wt %). The symmetry of Fe^{3+} species has been shown by means of XAFS to be octahedral.[29] Very recently, Fe/ZrO_2 calcined at 723 K has been briefly studied using Mössbauer spectroscopy.[30,31] A doublet peak observed at 77 K was tentatively assigned to paramagnetic Fe^{3+} ions at a low loading of Fe (0.8 wt % Fe). On the basis of

* Author to whom correspondence should be addressed. Fax: +81-852-32-6429. E-mail: yokamoto@riko.shimane-u.ac.jp.

† Department of Material Science, Shimane University.

‡ Department of Chemical Engineering, Faculty of Engineering Science, Osaka University.

§ Department of Physical Science, Graduate School of Engineering Science, Osaka University.

10.1021/jp994122t CCC: $19.00
Published on Web 08/12/2000

the room-temperature Mössbauer spectra for 3 wt % Fe/ZrO_2 calcined at 1023 K, Boot et al.[32] suggested the formations of α-Fe_2O_3 particles in a bimodal size distribution (< 7 nm and $\gg 12$ nm) and superparamagnetic Fe^{3+} species. FTIR studies[33,34] of CO and NO adsorbed on Fe/ZrO_2 (1 wt % Fe) reduced and subsequently outgassed at 623−773 K show the formation of highly dispersed FeO-like phase on the support. We have conducted a more systematic study on Fe/ZrO_2 calcined at 973 K as a function of Fe loading level using a variety of techniques including Mössbauer spectroscopy.[17] It is revealed that two kinds of highly dispersed Fe^{3+} species, catalytically active and inactive for NO−CO reaction, are formed as well as α-Fe_2O_3 particles.

In the present study, a 5 wt % Fe/ZrO_2 catalyst was characterized as a function of calcination temperature by means of ^{57}Fe Mössbauer and IR spectroscopies, XRD, and thermogravimetric analysis (TGA) techniques. It is disclosed that several kinds of Fe^{3+} species are formed on the surface of ZrO_2, depending on the calcination temperature. The nature of the interactions between Fe^{3+} species and the surface of ZrO_2 is discussed.

Experimental Section

Catalyst Preparation. A variety of 5 wt % Fe/ZrO_2 catalysts was prepared by impregnating ZrO_2 with aqueous solutions of $Fe(NO_3)_3 \cdot 9H_2O$ (0.8 cm^3 H_2O/g of ZrO_2).[13,17] After drying at 383 K for 20 h, the catalyst was calcined in air at a desired temperature (573−1373 K) for 1 h using an electric furnace. The catalyst is designated as Fe/ZrO_2, followed by calcination temperature (K), i.e., Fe/ZrO_2 (773) for 5 wt % Fe/ZrO_2 calcined at 773 K. ZrO_2 used here was provided by Daiichi-Kigenso Ltd., Japan (EP, BET surface area: 25 m^2 g^{-1}, Hf content: 1.38%).[14−17]

An amount of 2 wt % Fe/ZrO_2 was prepared by a coprecipitation technique. A solution of Na_2CO_3 was added to a mixed solution of $Fe(NO_3)_3$ and $ZrOCl_2$ at 293 K while vigorous stirring ($[Na_2CO_3]/([Fe(NO_3)_3] + [ZrOCl_2]) = 1.03$). The temperature of the resultant precipitates was raised to 348 K and held for 15 min, followed by filtration and washing with distilled water at 350 K. After drying at 383 K for 20 h, the precipitate was calcined at 973 K for 1 h. Aliquots of the sample were calcined again at 1173 K for 2 h or at 1373 K for 6 or 24 h.

Characterization. Mössbauer Spectroscopy. ^{57}Fe Mössbauer spectra were measured at 78 and 297 K using a spectrometer operated in a constant acceleration mode with a combination of velocity transducer, function generator, and power amplifier.[17,35] Spectra were stored using a multichannel analyzer operated in a multi-scaler mode. Every spectrum was analyzed using a thin foil approximation in which a least-squares fitting was carried out assuming Lorentian absorption lines. The isomer shift values are relative to α-Fe at 300 K.

Thermogravimetric Analysis (TGA). Thermogravimetric analysis of Fe/ZrO_2 (sample weight; ca. 50 mg) was conducted on a Shimazu DT-30 in a stream of N_2 (50 cm^3 min^{-1}). The temperature was raised from room temperature (RT) to 1083 K at a rate of 10 K min^{-1}. The weight decrease observed below 373 K was assumed to be caused by the desorption of physisorbed water.

IR and XRD. IR spectra of Fe/ZrO_2 were measured using an in situ cell at RT in a transmission mode on a Hitachi EPI-G spectrophotometer. The catalyst sample was pressed into a self-supporting disk (53−69 mg/20 mmϕ). The catalyst wafer was evacuated (ca. 10^{-5} Torr) at 573 K for 1 h and subsequently treated with 20 Torr of O_2 for 20 min at the temperature, followed by degassing for 1 min.

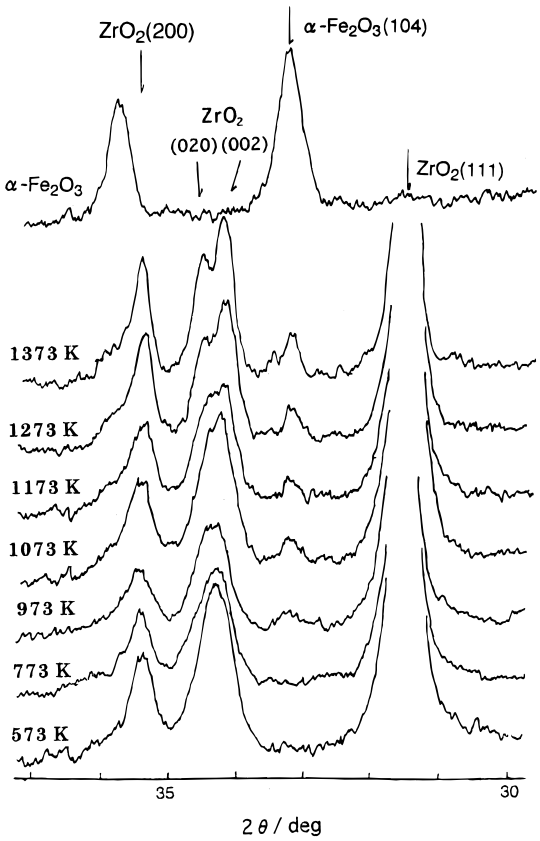

Figure 1. XRD patterns for 5 wt % Fe/ZrO_2 calcined at various temperatures.

X-ray powder diffraction (XRD) patterns of Fe/ZrO_2 were measured on a Shimazu VD-1 apparatus. The scan speed was 1° min^{-1}.

Reaction Procedure. NO−CO reaction was carried out using a fixed bed flow reactor made of quartz glass (outer diameter: 6 mmϕ, 0.1 g catalyst). The flow rate of the reaction gas was controlled by means of a mass flow meter (Ueshima−Brooks, 5850E). The concentrations of NO and CO were 2500 and 2000 ppm in a He stream (50 cm^3 min^{-1}, GHSV: ca. 30,000 h^{-1}). The reaction gas was periodically analyzed by means of an on-line gas chromatograph. The detailed procedures have been reported elsewhere.[17]

Results

X-ray Diffraction (XRD). Shown in Figure 1 are the XRD patterns of 5 wt % Fe/ZrO_2 as a function of calcination temperature. Only a narrow region of $2\theta = 30-37°$ is presented to examine the formation of α-Fe_2O_3 (hematite) ((104) at $2\theta = 33.3°$ and (110) at 35.7° PDF#01-1053). No formation of other Fe oxide or oxyhydroxide phases was detected by a wide scan XRD. Fe/ZrO_2 shows a diffraction pattern due to a monoclinic ZrO_2 phase ((111) at $2\theta = 31.5°$, PDF#36-0420) irrespective of the calcination temperature. No diffraction peaks due to a tetragonal ZrO_2 phase were detected. A broad peak at 34.3° becomes split into two peaks at 34.2 and 34.4° above 1173 K and more clearly splits as the calcination temperature increases further. These peaks are assigned to monoclinic ZrO_2 (002) and (020) diffractions, respectively. This evidently results from increasing crystallinity of the ZrO_2 support. A weak diffraction peak ascribed to α-Fe_2O_3 appears at $2\theta = 33.3°$ for Fe/ZrO_2-

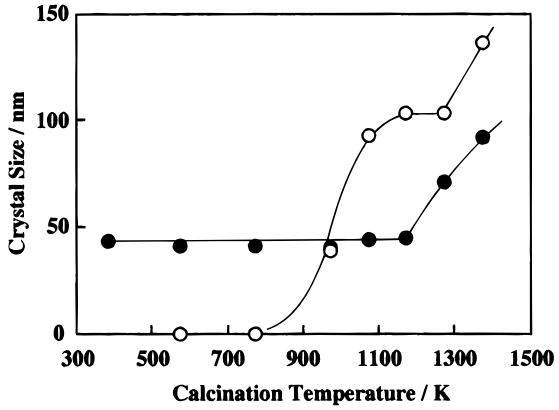

Figure 2. Crystalline sizes of monoclinic ZrO_2 (●) and α-Fe_2O_3 (○) in 5 wt % Fe/ZrO_2 as a function of calcination temperature.

(973) and grows as the calcination temperature increases above 973 K. A shoulder peak at 35.7° to α-Fe_2O_3 (110) also shows a similar behavior.

The crystallite sizes of monoclinic ZrO_2 and α-Fe_2O_3 are estimated from the line broadening of the diffraction peaks of ZrO_2 (111) (31.5°) and α-Fe_2O_3 (104) (33.3°) using the Sherrer equation (shape factor $K = 0.9$).[36] The instrumental line broadening was corrected using crystalline silicon powders. The crystalline sizes thus obtained are shown in Figure 2 against the calcination temperature. The crystallite size of ZrO_2 remains 41 ± 2 nm up to 1173 K, but it increases considerably above 1173 K. The surface area of the ZrO_2 is calculated from the crystallite size to be 26 $m^2\ g^{-1}$, in excellent agreement with the obserbed surface area (25 $m^2\ g^{-1}$). This indicates that the ZrO_2 has no porosity. The size of α-Fe_2O_3 crystals increases above 773 K and reaches about 100 nm at 1173−1273 K, followed by a further increase at a higher temperature. The BET surface area of Fe/ZrO_2 (measured by using N_2 adsorption at 77 K) was 25 ± 2 $m^2\ g^{-1}$, when the calcination temperature was lower than 1173 K, but it decreased to 3.8 $m^2\ g^{-1}$ on the calcination at 1373 K.

Mössbauer Spectroscopy. Mössbauer spectroscopy is particularly useful for the study of Fe catalysts.[37−40] Figure 3 shows room-temperature Mössbauer spectra obtained for the 5 wt % Fe/ZrO_2 catalysts calcined at various temperatures. The spectra are composed of a doublet component and a magnetically split sextet component. Chen et al.[31] reported similar spectra for 1.3 and 5.2 wt % Fe/ZrO_2 calcined at 723 K, but no Mössbauer parameters were given. The Mössbauer parameters for the present spectra are listed in Table 1. The isomer shift (IS) of the doublet peak is not varied very much by the calcination temperature and characteristic of Fe^{3+} species.[32,37−42] On the other hand, the quadrupole splitting (ΔEq) varies from 0.76 to 1.14 as the calcination temperature increases from 573 to 1373 K, indicating a change in the symmetry of the Fe^{3+} species. The Mössbauer parameters for the magnetically split sextet show no appreciable dependence on the calcination temperature.

Doublet components result from paramagnetic and/or superparamagnetic Fe species, while sextet components from Fe species in magnetically ordered states as anti-ferromagnet or ferromagnet.[37−42] In the present study, the former components include isolated Fe^{3+} species and/or highly dispersed Fe^{3+} oxide or oxyhydroxide species. The area fractions of the doublet and sextet components are determined from the spectra in Figure 3 and summarized in Table 1. They are presented in Figure 4 as a function of the calcination temperature. Before calcination, that is, after drying at 383 K for 20 h, all the Fe^{3+} species are in isolated and/or highly dispersed states. A doublet component

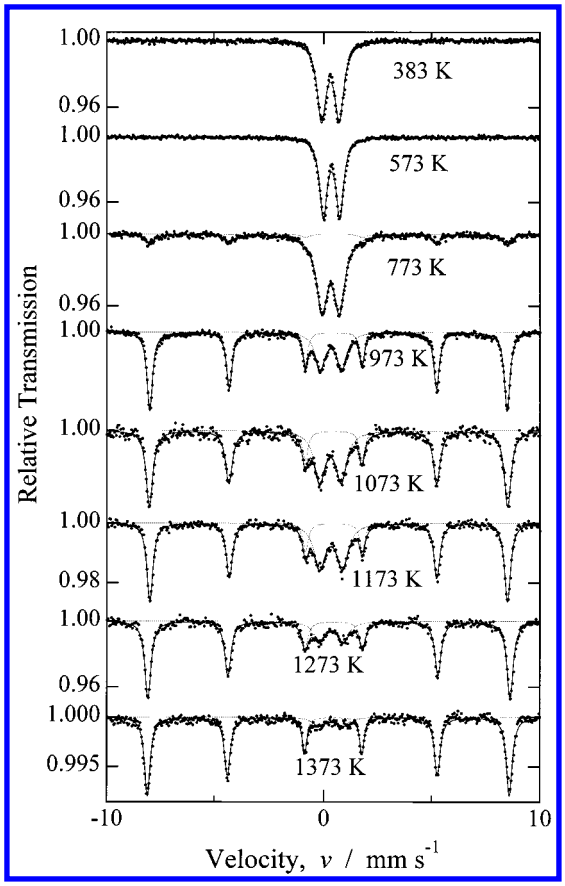

Figure 3. ^{57}Fe Mössbauer spectra measured at 297 K for 5 wt % Fe/ZrO_2 calcined at various temperatures.

dominates on Fe/ZrO_2 (573), too. The fraction of the doublet component considerably decreases above 773 K as the calcination temperature increases up to 973 K, followed by a slight increase and a subsequent decrease on a further rise in the calcination temperature from 973 to 1373 K. The area fraction of the sextet species changes in a reversed manner.

To obtain more detailed information on the Fe^{3+} species on Fe/ZrO_2, Mössbauer spectra were accumulated at 78 K and are shown in Figure 5. Obviously, the spectra for Fe/ZrO_2 calcined below 773 K are significantly changed by lowering the measurement temperature, while the spectra for Fe/ZrO_2 calcined above 973 K are essentially unchanged. The Mössbauer spectra for the catalysts calcined at the low temperature consist of a doublet component and broad sextet components. The latter components are indicative of the formation of magnetically split Fe^{3+} species having broad hyperfine field distribution. In the present study, the broad spectra were decomposed into a minimum number of sextet components, one for Fe/ZrO_2 (383) and (573) and three for Fe/ZrO_2 (773). The Mössbauer parameters of the respective components thus obtained are summarized in Table 2. On the basis of their broad features and deviations from the expected intensity ratio of 3:2:1:1:2:3, it should be noted that sextet (A) and (B) are composed of several Fe^{3+} species with different compositions and local structures. It is also established[39,41] that dynamic relaxation effects cause such unusual intensity ratios as well as broad peaks. It is not excluded at moment that the relaxation effects contribute, to some extent, to the Mössbauer spectra for Fe/ZrO_2 (383) and (573).

Figure 4 compares the area fractions of the doublet component and the sum of the sextet components calculated from the spectra obtained at 78 K with those obtained at 297 K. The fraction of

TABLE 1: Mössbauer Parameters Measured at 297 K for 5 wt % Fe/ZrO_2 Calcined at Various Temperatures for 1 h

calcination	doublet				sextet				
temperature/K	I/%	IS/mm s^{-1}	ΔEq/mm s^{-1}	FWHM/mm s^{-1}	I/%	IS/mm s^{-1}	ΔE'q/mm s^{-1}	Hi/kOe	FWHM/mm s^{-1}
383[a]	100	0.32	0.82	0.50					
573	100	0.38	0.76	0.41					
773	78	0.35	0.81	0.61	22	0.35	−0.23	512	0.52
973	30	0.33	0.98	0.53	70	0.37	−0.20	514	0.31
1073	33	0.33	0.99	0.60	67	0.38	−0.20	513	0.38
1173	34	0.36	1.04	0.63	66	0.39	−0.21	511	0.33
1273	18	0.37	1.11	0.64	82	0.37	−0.18	519	0.34
1373	9	0.34	1.14	0.72	91	0.35	−0.19	518	0.32
973[b]	100	0.29	1.02	0.81					
1173 (2)[b]	100	0.29	0.69	0.51					
1373 (6)[b]	74	0.30	0.67	0.53	26	0.17	0.13	482	0.38
1373 (24)[b]	82	0.26	0.64	0.55	18	0.18	0.02	480	0.46
α-Fe_2O_3					100	0.35	−0.21	517	0.37

[a] After drying for 20 h (uncalcined). [b] 2 wt % Fe/ZrO_2 prepared by a coprecipitation method, the numbers in parentheses; calcination time/h.

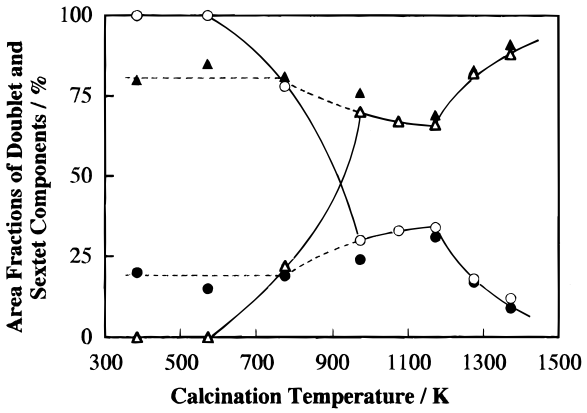

Figure 4. Area fractions of doublet and sextet components as a function of calcination temperature. (○) Doublet component, and (△) sextet component obtained from the Mössbauer spectra measured at 297 K. (●) Doublet component and (▲) sum of the sextet components obtained from the Mössbauer spectra measured at 78 K.

the doublet component remarkably decreases at 78 K for Fe/ZrO_2 calcined below 973 K. With Fe/ZrO_2 calcined above 973 K, however, the fractions of the doublet and sextet components are in excellent agreement with those observed at 297 K within the experimental error, ca. ±5% (Table 2).

As shown in Figure 5 and Table 2, there are, at least, "three" kinds of sextet components. Sextet (A) (Table 2) is preferentially observed for Fe/ZrO_2 calcined below 573 K. When Fe/ZrO_2 is calcined at 773 K, a new sextet, sextet (B), appears, at the expense of sextet (A), together with sextet (C), which becomes predominating on Fe/ZrO_2 (973). Accordingly, it is considered that sextet (A) originally produced after drying transforms to sextet (C) through sextet (B) as intermediate Fe^{3+} species. The fraction of the doublet component remains constant below 773 K and gradually increases as the calcination temperature increases further to reach a maximum around 1100 K. It is considered that the incremental doublet component between the calcination temperatures of 773 and 973 K is evidently produced from sextet (A) or (B) during the calcination.

Figure 6 shows the Mössbauer spectra measured at 297 K for 2 wt % Fe/ZrO_2 prepared by a coprecipitation method. The Mössbauer parameters are presented in Table 1. With 2 wt % Fe/ZrO_2 calcined above 1173 K, the quadrupole splitting ΔEq for the doublet component is considerably smaller than those for the doublet components observed for 5 wt % Fe/ZrO_2. In addition, the parameters of the sextet components in 2 wt % Fe/ZrO_2 are also different from those for 5 wt % Fe/ZrO_2 and α-Fe_2O_3. These results indicate that the doublet and sextet

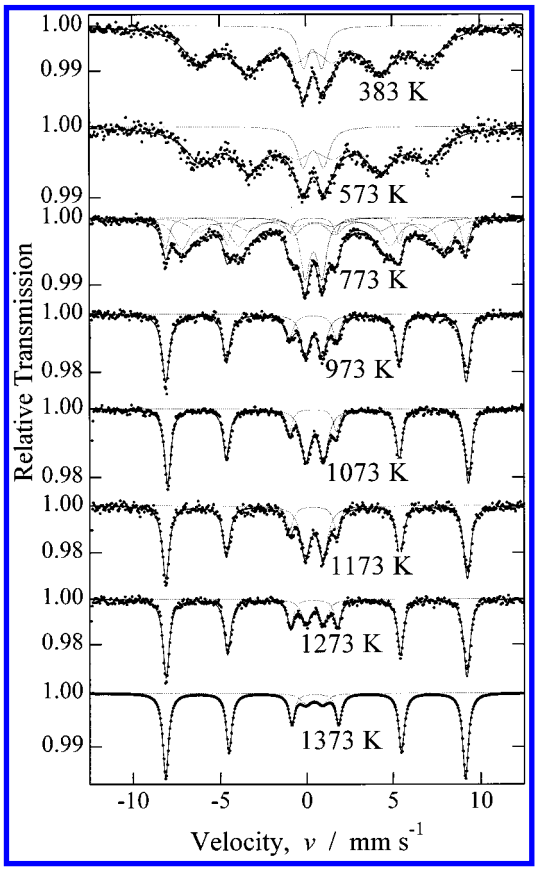

Figure 5. Mössbauer spectra measured at 78 K for 5 wt % Fe/ZrO_2 calcined at various temperatures.

species in 2 wt % Fe/ZrO_2 prepared by a coprecipitation method are different from those in the impregnation catalysts, 5 wt % Fe/ZrO_2.

IR Spectroscopy. Figure 7 shows the IR spectra of the OH region for Fe/ZrO_2 and ZrO_2. ZrO_2 shows three OH bands at 3776, 3674, and 3734 cm^{-1}, as shown previously.[14,15] The former two bands are attributed to terminal and bridged OH species on the surface of ZrO_2, respectively,[43] and the last one to the OH groups attached to impurity HfO_2.[14,15] It is noted that Fe/ZrO_2 shows significantly weaker IR bands than ZrO_2, indicating that the surface OH groups are extensively consumed on the addition of 5 wt % Fe. On the basis of the IR band intensities ($\log(I_0/I)$ normalized to the surface area of ZrO_2 in the sample), it is estimated that about 65% of the OH groups are lost for Fe/ZrO_2 (573). The band intensity gradually decreases as the calcination temperature increases. In the present

TABLE 2: Mössbauer Parameters Measured at 78 K for 5 wt % Fe/ZrO_2 Calcined at Various Temperatures for 1 h

Fe component		calcination temperature/K							
		383[a]	573	773	973	1073	1173	1273	1373
doublet	*I*/%	20 ± 6	15 ± 6	19 ± 3	24 ± 3	33 ± 6	31 ± 6	17 ± 6	9 ± 3
	FWHM/mm s^{-1}	0.70 ± 0.04	0.82 ± 0.24	0.65 ± 0.06	0.60 ± 0.09	0.65 ± 0.06	0.65 ± 0.03	0.61 ± 0.12	0.77 ± 0.48
	IS/mm s^{-1}	0.47 ± 0.03	0.43 ± 0.06	0.43 ± 0.03	0.43 ± 0.01	0.47 ± 0.03	0.44 ± 0.03	0.45 ± 0.01	0.42 ± 0.12
	ΔEq/mm s^{-1}	1.04 ± 0.03	1.21 ± 0.18	0.98 ± 0.03	1.00 ± 0.02	1.04 ± 0.01	1.05 ± 0.02	1.02 ± 0.03	0.97 ± 0.24
sextet (A)	*I*/%	80 ± 6	85 ± 6	23 ± 3					
	FWHM/mm s^{-1}	2.07 ± 0.15	2.07 ± 0.21	1.40 ± 0.39					
	IS/mm s^{-1}	0.44 ± 0.03	0.48 ± 0.06	0.43 ± 0.09					
	ΔEq/mm s^{-1}	−0.08 ± 0.06	−0.05 ± 0.06	−0.09 ± 0.05					
	Hi/kOe	410 ± 3	407 ± 6	409 ± 12					
sextet (B)	*I*/%			41 ± 3					
	FWHM/mm s^{-1}			1.14 ± 0.24					
	IS/mm s^{-1}			0.45 ± 0.03					
	ΔEq/mm s^{-1}			−0.06 ± 0.06					
	Hi/kOe			471 ± 3					
sextet (C)	*I*/%			17 ± 3	76 ± 3	67 ± 6	69 ± 6	83 ± 6	91 ± 3
	FWHM/mm s^{-1}			0.47 ± 0.09	0.50 ± 0.03	0.44 ± 0.03	0.48 ± 0.03	0.43 ± 0.03	0.39 ± 0.03
	IS/mm s^{-1}			0.46 ± 0.03	0.46 ± 0.01	0.50 ± 0.01	0.46 ± 0.01	0.46 ± 0.01	0.48 ± 0.01
	ΔEq/mm s^{-1}			0.12 ± 0.03	0.16 ± 0.01	0.28 ± 0.03	0.28 ± 0.03	0.19 ± 0.03	0.01 ± 0.03
	Hi/kOe			536 ± 3	537 ± 1	537 ± 1	539 ± 1	539 ± 1	536 ± 1

[a] After drying for 20 h (uncalcined).

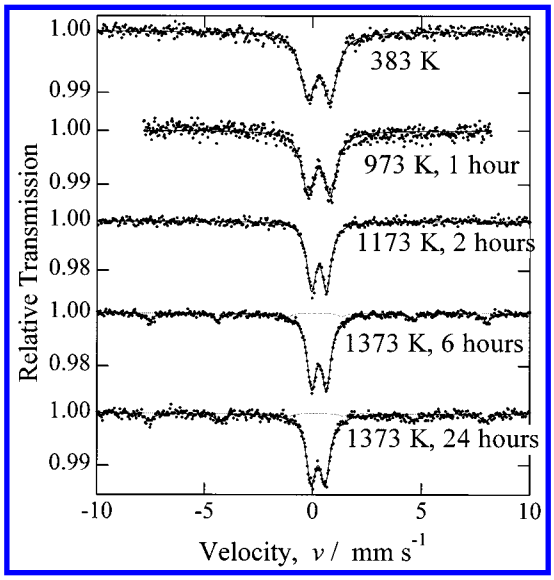

Figure 6. Mössbauer spectra measured at 297 K for 2 wt % Fe/ZrO_2 prepared by a coprecipitation method. The calcination temperature (K) and time (h) are varied.

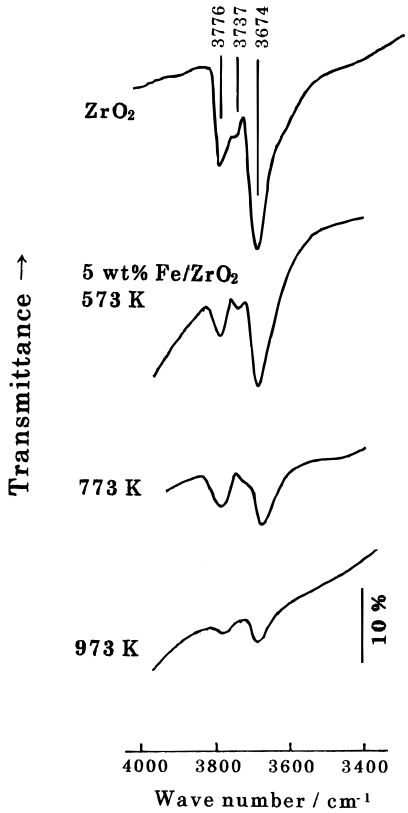

Figure 7. IR spectra of the OH bands for 5 wt % Fe/ZrO_2 calcined at various temperatures. Sample weight; ZrO_2: 54.1 mg, Fe/ZrO_2 (573): 65.1 mg, Fe/ZrO_2 (773): 68.7 mg and Fe/ZrO_2 (973): 52.8 mg.

IR study, no residual NO_3^- anions (ca. 1400 cm^{-1})[44] were detected even on Fe/ZrO_2 (573).

Thermogravimetric Analysis (TGA). The dehydration behavior of Fe/ZrO_2 was examined by using a TGA technique. Shown in Figure 8 are the TGA profiles for Fe/ZrO_2. With Fe/ZrO_2 calcined above 773 K and ZrO_2, the weight gradually decreases as the sample temperature is raised, while the maximum rates of the weight loss are observed at 475 and 600 K for Fe/ZrO_2 (383) and Fe/ZrO_2 (573), respectively. It is considered that the decrease in weight ΔW^0 between 373 and 973 K is caused by the decompositions of Fe^{3+} oxyhydroxides and nitrates and by the dehydration of residual surface OH groups, assuming that the weight loss due to the desorption of physisorbed water is completed by 373 K. The weight loss ΔW^0 normalized to the catalyst weight W, $\Delta W^0/W$, is summarized in Table 3. Obviously, with increasing calcination temperature, the normalized weight loss decreases steeply, followed by only a small weight loss above 773 K. In the case of the ZrO_2 support, a weight loss of 0.40 wt % is observed between 373 and 973 K. Assuming that the weight loss of ZrO_2 is caused by the dehydroxylation of the surface OH groups, the surface density of the OH groups is calculated to be 11 OH nm^{-2}. This value may indicate that the surface of ZrO_2 is fully hydroxylated.

Catalytic Activity of Fe/ZrO_2. The catalytic behavior of Fe/ZrO_2 (973) has been reported elsewhere as a function of Fe loading level.[13,17] Analogous observations were made for 5 wt % Fe/ZrO_2 catalysts calcined at various temperatures. The rate equation has been found to be expresses as follows:[17]

$$r = k_{NO} P_{CO}^{0.9} P_{NO}^{-0.4}$$

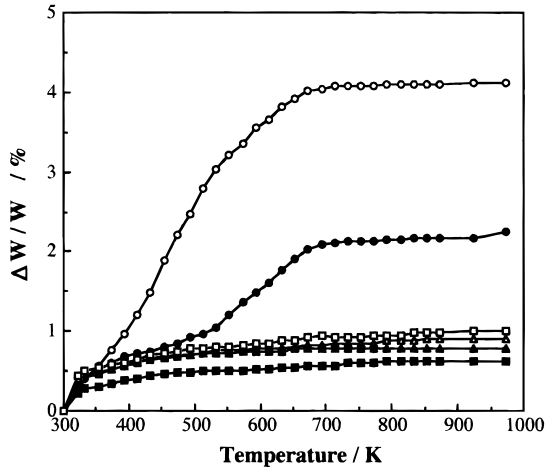

Figure 8. TGA profiles of 5 wt % Fe/ZrO_2 calcined at various temperatures. The weight loss ΔW is normalized to the sample weight W. Calcination temperature; ○: 383 K (20 h), ●: 573 K, △: 773 K, ▲: 973 K and ■: 1173 K. The TGA profile of ZrO_2 is included for comparison (□).

TABLE 3: Thermogravimetric Analysis of 5 wt % Fe/ZrO_2 Calcined at Various Temperatures for 1 h

calcination temperature/K	$\Delta W^0/W/\%$[a]
383[b]	3.40
573	1.75
773	0.36
973	0.24
1173	0.25
ZrO_2[c]	0.40

[a] Weight loss ΔW^0 between 373 and 973 K normalized to the sample weight W. [b] After drying at 383 K for 20 h. [c] ZrO_2 without supported Fe.

TABLE 4: Rate Constant of NO−CO Reaction[a] at 523 K over Fe/ZrO_2 as a Function of Calcination Temperature

calcination temperature/K	rate constant k_{NO}[b]
573	83.5
773	63.1
973	16.2
1073	13.2
1173	7.5
1273	0.2
1373	0.003

[a] P_{CO} = 2000 ppm and P_{NO} = 2500 ppm, GHSV; ca. 30000 h^{-1}. [b] 10^{-7} mol s^{-1} g-cat^{-1} $Pa^{-0.5}$.

where k_{NO} is a rate constant. P_{CO} and P_{NO} represent the partial pressures of CO and NO, respectively, in the reaction gas. The value of k_{NO} obtained at 523 K is listed in Table 4. The accuracy of k_{NO} is estimated to be ±5% except for the values for Fe/ZrO_2 (573) and (773) (about ±10%). Fe/ZrO_2 (573) shows an extremely high activity for the NO−CO reaction. The activity of Fe/ZrO_2, however, decreases with increasing calcination temperature and becomes very low upon the calcination above 1273 K. A comparison of the activity with the Mössbauer results in Table 2 indicates that the activity is not delineated to a single Fe^{3+} species in the catalyst.

Discussion

In our separate study[17] on Fe/ZrO_2 (973), it has been shown that Fe species depend on the Fe content and that two kinds of (super)paramagnetic or highly dispersed Fe^{3+} species, catalytically active and inactive for NO−CO reaction, and α-Fe_2O_3 are formed, the highly dispersed species being predominant below 2 wt % Fe. The present physicochemical characterization techniques, in particular Mössbauer technique clearly indicate that the interaction modes between Fe^{3+} species and the surface of ZrO_2 strongly depend on the calcination temperature. The Fe species formed on 5 wt % Fe/ZrO_2 will be discussed separately in two calcination temperature regions, below and above 973 K.

Iron Species Formed below 973 K. When Fe/ZrO_2 is calcined below 973 K, the crystal structure of the ZrO_2 support employed here is of a monoclinic form (crystal size; 41 nm). The unresolved (020) and (002) diffraction peaks in Figure 2 are suggestive of the presence of a considerable amount of defects in the ZrO_2 lattice. The crystalline properties of the ZrO_2 support as well as the surface area are not affected by the calcination below 973 K. The ZrO_2 support has no porosity.

The Mössbauer results in Figure 5 clearly show the formations of at least "four" kinds of Fe^{3+} components on Fe/ZrO_2: sextet (A), (B), and (C) and (super)paramagnetic Fe^{3+} component. Magnetically split component (C) has a narrow spectral width (Table 2). It is readily assigned to α-Fe_2O_3 on the basis of the Mössbauer parameters, in agreement with the XRD results in Figure 1. Sextet (A) and (B) show superparamagnetism at 297 K, indicating that these components stem from highly dispersed Fe^{3+} species which are in magnetically ordered states at 78 K. The broad spectral features of sextet (A) and (B) obviously indicate that these components involve several Fe^{3+} species having slightly different compositions and local structures. It is considered from the changes in the fraction of the Fe^{3+} components in Table 2 that sextet (A) is stable at 573 K but transforms at 773 K to sextet (B) and α-Fe_2O_3. Finally, sextet (A) and (B) disappear at 973 K to form (super)paramagnetic Fe^{3+} component and α-Fe_2O_3. The changes in the fractions of sextet (A) and (B) with the calcination temperature may suggest that major parts of the incremental doublet component and α-Fe_2O_3 on Fe/ZrO_2 (973) are produced from sextet (A) via sextet (B) as an intermediate Fe^{3+} species.

The stoichiometry of the Fe^{3+} species presented by sextet (A) is estimated from the TGA results in Table 3. When $Fe(NO_3)_3$ is decomposed to Fe_2O_3, a weight loss of 14.5 wt % is expected for 5 wt % Fe/ZrO_2. In the cases of $Fe(OH)_3$ (or $FeOOH{\cdot}H_2O$) and FeOOH, 2.4 and 0.81 wt % of the weight are calculated to decrease, respectively, during the decompositions to Fe_2O_3. The observed weight loss of 3.4 wt % for Fe/ZrO_2 (383) suggests that the decomposition of NO_3^- anions is almost completed even after drying, in agreement with the IR results showing the absence of a band[44] around 1400 cm^{-1} characteristic of NO_3^- anions. With Fe/ZrO_2 (573), the weight loss due to the dehydroxylation of the ZrO_2 support is expected to be very small (35% of 0.40 wt % or 0.14 wt %), since 65% of the surface OH groups is consumed by the impregnation of 5 wt % Fe, according to the IR results. Accordingly, the observed weight loss of 1.75 wt % for Fe/ZrO_2 (573) suggests that major Fe^{3+} species are composed of partially hydrated oxyhydroxide species $FeOOH{\cdot}nH_2O$ ($n < 1$). The degree of hydration, n, varies in the hydroxides to provide a broad hyperfine distribution of the magnetically split component. The Mössbauer results indicate that analogous species predominate after drying at 383 K. The Mössbauer parameters in Tables 1 and 2 are in good agreement with the formation of $FeOOH{\cdot}nH_2O$ species.[38,45] Taking into account that sextet (A) shows superparamagnetism at RT, it is concluded that sextet (A) is assigned to partially hydrated FeOOH fine particles.

Generally, high-spin Fe^{3+} is an S state ion and shows very small ΔEq value. Fe^{3+} species in an octahedral symmetry show

slightly larger IS values compared with Fe^{3+} species in a tetrahedral symmetry because of its higher ionic bondings.[40,42] In the case of a tetrahedral symmetry, Fe^{3+} species are more covalent and show larger ΔEq values. Intermediate ($S = 3/2$) or low-spin ($S = 1/2$) Fe^{3+} states should show rather large ΔEq values because of the nonspherical distribution of the valence electrons. It is considered from the ΔEq values (ca. 0.8 mm s^{-1}) in Table 1 for the doublet component at 297 K that the Fe^{3+} species on Fe/ZrO_2 (383) and Fe/ZrO_2 (573) are in a distorted octahedral symmetry, since the values are close to those observed for Fe^{3+} species in octahedral coordinations (IS$\sim$0.39 mm s^{-1}, ΔEq$\sim$0.64 mm s^{-1}) rather than those in tetrahedral ones (IS $\sim$ 0.21 mm s^{-1}, ΔEq $\sim$ 1.29 mm s^{-1}).[42,46] This is consistent with the assignment of sextet (A).

A weight loss of 0.36 wt % observed for Fe/ZrO_2 (773) suggests that oxyhydroxide species (A) are considerably decomposed during the calcination at 773 K to produce sextet (B) and α-Fe_2O_3. The broad feature of sextet (B) suggests broad distributions of the composition and local structure of magnetically split Fe^{3+} species, as discussed for sextet (A). Since the apparent Mössbauer parameters of sextet components (A) and (B) are very close to each other (Table 2), sextet (B) may be attributed to partially dehydrated FeOOH species, $FeO_n(OH)_{3-2n}$ ($n < 1$), in a highly dispersed state as fine particles. With Fe/ZrO_2 (973), α-Fe_2O_3 particles of 40 nm in size predominate (70−76% of Fe) as indicated by XRD and Mössbauer spectroscopy, in conformity with the TGA results showing the formation of Fe_2O_3 as a major species.

In addition to the superparamagnetic and magnetically split components, Fe^{3+} species paramagnetic at 78 K are formed in Fe/ZrO_2 even after drying. The amount of the paramagnetic Fe^{3+} species is not changed by calcination below 773 K and is calculated to be 0.90 $\pm$ 0.08 wt % Fe on the basis of the spectral intensities and loading level of Fe (Table 2), assuming that the spectral intensity is proportional to the Fe content. The IR results indicate that a significant fraction of the surface OH groups of ZrO_2 is consumed on the impregnation of 5 wt % Fe. In our previous work[17] on Fe/ZrO_2 (973) having various Fe loading levels, it has been shown that paramagnetic Fe^{3+} species of 0.65 wt % Fe, which are preferentially formed at a low Fe content, extensively consume the surface OH groups. Accordingly, it is inferred that the paramagnetic Fe^{3+} species on Fe/ZrO_2 calcined below 773 K are formed by ion-exchange with the surface OH groups. It is considered that the paramagnetic Fe^{3+} species produced by ion-exchange are stabilized on the surface of ZrO_2 by forming $Fe^{3+}-O-Zr^{4+}$ bondings. Taking into consideration the number of consumed surface OH groups on ZrO_2 (65% of 11 OH nm^{-2} or 7.2 OH nm^{-2}) estimated from the TGA and IR experiments and the amount of the paramagnetic Fe^{3+} species (0.90 $\pm$ 0.08 wt % Fe or 4.0 $\pm$ 0.3 Fe nm^{-2}), it is considered that the number of the consumed OH groups per paramagnetic Fe^{3+} species is 1.8 $\pm$ 0.2 OH/Fe^{3+}. It has been reported[15,25] that Cu^{2+} ions are supported on ZrO_2 by ion-exchange. The Mössbauer parameters in Table 2 indicate that these species are in distorted octahedral coordinations, in conformity with the XAFS results by Yamamoto et al.[29] As shown previously,[17] the ion-exchanged Fe^{3+} species are catalytically inactive for NO−CO reaction at 523 K.

The amount of the paramagnetic component increases as the calcination temperature increases beyond 773 K and reaches 1.6 wt % Fe after the calcination at 1073 K. The paramagnetic Fe^{3+} species formed above 773 K accompany no extensive consumption of the surface OH groups as shown in Figure 7. From the dependencies of the amounts of the sextet species on the calcination temperature, it is considered that the incremental paramagnetic species formed above 773 K are produced by the dehydration of Fe^{3+} oxyhydroxides. These species are tentatively attributed to Fe^{3+} oxide clusters, whose size is small enough to show superparamagnetism at 78 K. According to Kündig et al.,[47] the cluster size is calculated to be well below 8 nm.[17] The total amount of the paramagnetic species is maximized at 1.6 wt % Fe for Fe/ZrO_2 (1073), which is close to the value of 1.4 wt % Fe observed for 5−8 wt % Fe/ZrO_2 (973).[17] On the basis of a correlation between k_{NO} and the amount of (super)paramagnetic Fe^{3+} species, it has been concluded that the highly dispersed Fe^{3+} species produced without extensive consumption of the surface OH groups are responsible for NO−CO reaction.[17] Accordingly, it is concluded that the superparamagnetic Fe^{3+} oxide clusters, produced by the decomposition of the fine oxyhydroxide particles (sextet (A) and (B)), show a high activity for NO−CO reaction. The Fe^{3+} species proposed for 5 wt % Fe/ZrO_2 are schematically illustrated in Figure 9. In the present study, it is not evident whether the ion-exchanged Fe^{3+} species are present as a separate phase or associated with the interfaces

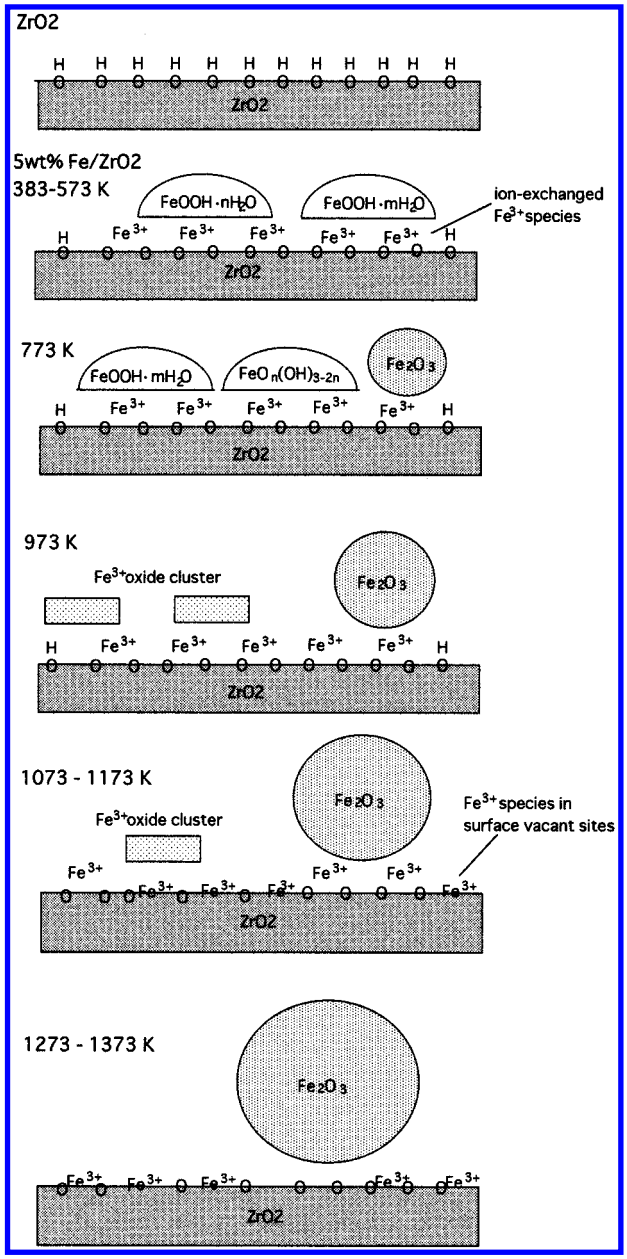

Figure 9. Schematic model of 5 wt % Fe/ZrO_2 as a function of calcination temperature.

between hydrated or dehydrated FeOOH fine particles and the ZrO_2 surface.

Iron Species Formed above 973 K. The crystallinity of the ZrO_2 support increases as the calcination temperature increases above 1173 K as evidenced by the improved resolution of ZrO_2 (002) and (020) diffraction peaks in Figure 1. In addition, the surface area of Fe/ZrO_2 decreases when Fe/ZrO_2 is calcined above 1173 K. The XRD and Mössbauer results indicate the formation of crystalline α-Fe_2O_3, whose size increases with increasing calcination temperature (Figure 2). Furthermore, with Fe/ZrO_2 calcined above 973 K, the fractions of α-Fe_2O_3 and the doublet component are not changed by the measurement temperature of the Mössbauer spectra, as shown in Figure 4. It is noteworthy that essentially no superparamagnetic Fe^{3+} species having a transition temperature between 78 and 297 K are present on Fe/ZrO_2 calcined above 973 K. In contrast to the present preparations, Boot et al.[32] have claimed a bimodal Fe oxide distribution for 3 wt % Fe/ZrO_2 calcined at 1023 K, on the basis of the RT- Mössbauer spectra showing two kinds of sextet components with different hyperfine splittings (Hi).

The fraction of the paramagnetic component increases as the calcination temperature increases and reaches a maximum around 1100 K, followed by a subsequent decrease above 1273 K. The fraction of α-Fe_2O_3 changes in a reversed fashion above 973 K. These results strongly suggest the changes in the nature of the paramagnetic species with the calcination temperature. When the calcination temperature is lower than 773 K, the paramagnetic species are formed by ion-exchange with the surface OH groups of ZrO_2. The superparamagnetic Fe^{3+} oxide clusters are concluded to originate from Fe^{3+} oxyhydroxides between 773 and 973 K, as discussed above. The ΔEq value in Table 1 steadily increases from 0.98 to 1.14 mm s^{-1} as the calcination temperature increases from 973 to 1373 K, indicating the formation of new paramagnetic species in a lower symmetry. We propose that the increase in the fraction of the paramagnetic component above 973 K is caused by trapping of Fe^{3+} ions in surface vacant sites of ZrO_2, since Fe^{3+} cations dissolved in a ZrO_2 lattice show Mössbauer parameters completely different from those observed for Fe/ZrO_2 calcined above 973 K, as discussed below. When the calcination temperature of Fe/ZrO_2 increases above 1173 K, the fraction of the paramagnetic component decreases. Taking into consideration the decreasing surface area and increasing crystallinity of ZrO_2 in this temperature range, it is concluded that the Fe^{3+} ions trapped in surface vacant sites are agglomerated above 1173 K on the surface of ZrO_2 particles to form large crystalline α-Fe_2O_3 particles, whose formation is evidenced by the XRD results in Figure 2. The surface concentration of the Fe^{3+} ions is maximized at 1373 K (13 Fe nm^{-2}). A proposed surface model of Fe/ZrO_2 is schematically presented in Figure 9.

A formation of solid solutions of monoclinic ZrO_2−Fe_2O_3 was reported by Collins et al.[48] for the samples prepared by a coprecipitation technique and calcined at 1173 K for 12 h. The extent of dissolution was estimated by XRD to be 20 mol % Fe in ZrO_2. To obtain more detailed information on the dissolution and segregation behavior of Fe^{3+} species, 2 wt % Fe/ZrO_2 prepared by coprecipitation and calcined at 973−1373 K was studied by Mössbauer spectroscopy at 297 K. As shown in Figure 6, only a doublet component is observed, when the calcination temperature is lower than 1173 K. The fraction of the doublet component slightly decreases at 1373 K to form magnetically ordered species. The ΔEq value for the doublet component decreases between the calcination temperatures of 973 and 1173 K, followed by a gradual decrease at a higher temperature or for a longer calcination time. The ΔEq value for 2 wt % Fe/ZrO_2 calcined above 1173 K is considerably small, at which temperature Fe^{3+} cations are considered to be dissolved in the ZrO_2 phase.[48] The parameters indicate that paramagnetic Fe^{3+} species are in an octahedral symmetry in conformity with the dissolution of Fe^{3+} cations in the ZrO_2 lattice. A comparison of these Mössbauer parameters with those for 5 wt % Fe/ZrO_2 calcined above 1173 K leads us to propose the formation of the Fe^{3+} species trapped in the surface vacant sites of ZrO_2 for 5 wt % Fe/ZrO_2 rather than Fe^{3+} species dissolved in the ZrO_2 lattice.

The Mössbauer parameters for the sextet species in 2 wt % Fe/ZrO_2 are considerably different from those for α-Fe_2O_3 observed for the 5 wt % Fe/ZrO_2 impregnation catalysts. The magnetically split species in 2 wt % Fe/ZrO_2 are assigned to fine particles of α-Fe_2O_3 (<7 nm)[49] or to mixed oxides of ZrO_2 and Fe_2O_3.

Catalytically Active Species on Fe/ZrO_2 for NO−CO Reaction. In our separate study[17] on Fe/ZrO_2 (973), it has been found that the Fe^{3+} oxide clusters are catalytically active for NO−CO reaction, while ion-exchanged Fe^{3+} paramagnetic species and α-Fe_2O_3 are much less active at 523 K. The activity of Fe/ZrO_2 decreases as the calcination temperature increases and becomes inactive when calcined at 1273 K, although the amount of (super)paramagnetic Fe^{3+} species shows a maximum around 1100 K. As discussed above, this results from the change in the nature of the (super)paramagnetic species with the calcination temperature. The catalytically active superparamagnetic Fe^{3+} oxide clusters are gradually consumed by a reaction with ZrO_2 to form the Fe^{3+} species in the surface vacant sites and by sintering to form α-Fe_2O_3, as the calcination temperature increases above 973 K. The active Fe^{3+} clusters are entirely lost at 1273 K. Since the paramagnetic species in Fe/ZrO_2 calcined above 1273 K are mainly composed of the Fe^{3+} cations in the surface vacant sites, it is inferred that these species are inactive for the reaction at 523 K. On the other hand, it is shown that (partially) dehydrated FeOOH species show a very high activity for the NO−CO reaction.

Conclusions

In the present study, 5 wt % Fe/ZrO_2 was characterized by means of ^{57}Fe Mössbauer spectroscopy, IR, XRD, and thermogravimetric analysis (TGA) to reveal the metal oxide−support interactions in ZrO_2-supported Fe oxide catalysts as a function of calcination temperature. It is shown that when Fe/ZrO_2 is calcined below 573 K, small particles of hydrated Fe^{3+} oxyhydroxides (superparamagnetic at 297 K) are formed together with paramagnetic Fe^{3+} cation species ion-exchanged with the surface OH groups of ZrO_2. In addition to the Fe^{3+} ion-exchanged species, Fe^{3+} oxide clusters and crystalline α-Fe_2O_3 particles are formed by successive dehydration of the oxyhydroxides on calcination at 973 K. The Mössbauer spectroscopic results suggest that Fe^{3+} cation species trapped in surface vacant sites of ZrO_2 are formed at the expense of the Fe^{3+} oxide clusters, when Fe/ZrO_2 is calcined at 1073 or 1173 K. When Fe/ZrO_2 is calcined at a higher temperature, crystalline α-Fe_2O_3 predominates with a small amount of the Fe^{3+} cations in the vacant sites. With 2 wt % Fe/ZrO_2 prepared by a coprecipitation method and calcined at 1173−1373 K, Fe^{3+} cations dissolved in a ZrO_2 lattice predominate.

Acknowledgment. We are grateful to Dr. S. Tsutsui (Japan Atomic Energy Research Institute) for useful discussions.

References and Notes

(1) Knözinger, H. *Proc. 9th Int.Congr. Catal., Calgary* **1988**, *5*, 20.

(2) Boehm, H. P.; Knözinger, H. *Catalysis-Science and Engineering*; Anderson, J. R., Boudard, M., Eds.; Springer-Verlag: Berlin, 1983; Vol. 4, p 39.
(3) Iwasawa, Y. *Tailored Metal Catalysts*; Iwasawa, Y., Ed.; Reidel: Dordrecht, 1986; p 1.
(4) Massoth, F. E. *Adv. Catal*. **1978**, *27*, 292.
(5) Chan, S. S.; Wachs, I. E.; Murrel, L.; Dispenziere, N. C. *J. Catal*. **1985**, *92*, 1.
(6) Bruggref, L. W.; Leyden, D. E.; Chin, R. L.; Hercules, D. M. *J. Catal*. **1982**, *78*, 360.
(7) Okamoto, Y.; Imanaka, T. *J. Phys. Chem*. **1988**, *92*, 7102.
(8) Chen, Y.; Zhang, L. *Catal. Lett*. **1992**, *12*, 51.
(9) Gao, X.; Bare, S. R.; Weckhyusen, B. W.; Wachs, I. E. *J. Phys. Chem. B* **1998**, *102*, 10842.
(10) Chernavskii, P. A.; Lunin, V. V. *Kinet. Catal*. **1993**, *34*, 470.
(11) Yamaguchi, T. *Catal. Today* **1994**, *20*, 199.
(12) Yamaguchi, T.; Tanno, M.; Tanabe, K. *Stud. Surf. Sci. Catal*. **1991**, *63*, 567.
(13) Okamoto, Y.; Ohto, Y.; Imanaka, T. *Kagaku Kogaku Ronbunshu* **1993**, *19*, 863.
(14) Okamoto, Y.; Gotoh, H. *Catal. Today* **1997**, *36*, 71.
(15) Okamoto, Y.; Gotoh, H.; Aritani, H.; Tanaka, T.; Yoshida, S. *J. Chem. Soc., Faraday Trans.* **1997**, *93*, 3879.
(16) Okamoto, Y.; Kubota, T.; Gotoh, H.; Ohto, Y.; Aritani, H.; Tanaka, T.; Yoshida, S. *J. Chem. Soc., Faraday Trans.* **1998**, *94*, 3743.
(17) Okamoto, Y.; Kubota, T.; Ohto, Y.; Nasu, S. *J. Catal*. **2000**, *192*, 412.
(18) Boot, L. A. Ph.D. Thesis, Utrecht University, 1994.
(19) Mizuno, N.; Yamamoto, M.; Tanaka, M.; Misono, M. *Bull. Chem. Soc. Jpn*. **1991**, *64*, 1383.
(20) Mizuno, N.; Yamamoto, M.; Tanaka, M.; Misono, M. *J. Catal*. **1991**, *132*, 560.
(21) Hsu, C. Y.; Heimbuch, C. R.; Armes, C. T.; Gates, B. C. *J. Chem. Soc., Chem. Commun.* **1992**, 1645.
(22) Jatia, A.; Chan, C.; MacLeod, J. D.; Okubo, T.; Davis, M. E. *J. Catal*. **1994**, *25*, 21.
(23) Wan, K. T.; Khouw, C. B.; Davis, M. E. *J. Catal*. **1996**, *158*, 311.
(24) Cheung, T. C.; Gates, B. C. *Top. Catal.* **1998**, *6*, 41.
(25) Shimokawabe, M.; Arakawa, H.; Takezawa, N. *Appl. Catal*. **1990**, *59*, 45.
(26) Dow, W.; Huang, T. *J. Catal*. **1994**, *147*, 322.
(27) Mizuno, N.; Fujii, H.; Igarashi, H.; Misono, M. *J. Am. Chem. Soc*. **1992**, *114*, 7151.
(28) Ji, W.; Kuo, Y.; Shen, S.; Li, S.; Wan, H. *Proc. 10th Intern. Congr. Catal., Budapest* **1992**, 2059.
(29) Yamamoto, H.; Tanaka, T.; Takenaka, S.; Yoshida, S.; Onari, T.; Takahashi, Y.; Kosaka, T.; Hasegawa, S.; Kudo, M. *J. Phys. Chem. B* **1999**, *103*, 2385.
(30) Chen, K.; Fan, Y.; Hu, Z.; Yan, Q. *Catal. Lett*. **1996**, *36*, 139.
(31) Chen, K.; Dong, L.; Yan, Q.; Chen, Y. *J. Chem. Soc., Faraday Trans*. **1997**, *93*, 2203.
(32) Boot, L. A.; van Dillen, A. J.; Geus, J. W.; van der Kraan, A. M.; van der Horst, A. A.; van Buren, F. R. *Appl. Catal. A* **1996**, *145*, 389.
(33) Guglielminotti, E. *J. Phys. Chem*. **1994**, *98*, 4884.
(34) Guglielminotti, E. *J. Phys. Chem*. **1994**, *98*, 9033.
(35) Nasu, S.; Shimizu, S. *J. Catal*. **1987**, *104*, 164.
(36) Gallezot, P. In *Catalysis-Science and Technology*; Anderson, J. R., Boudart, M., Eds.; Springer-Verlag: Berlin, 1984; Vol. 5, p 221.
(37) Delgass, W. N.; Boudart, M. *Catal. Rev.−Sci. Eng*. **1968**, *2*, 129.
(38) Gager, H. M.; Hobson, M. C., Jr. *Catal. Rev.−Sci. Eng*. **1975**, *11*, 17.
(39) Dumesic, J. A.; Topsøe, H. *Adv. Catal.* **1977**, *26*, 121.
(40) Delgass, W. N.; Haller, G. L.; Kellerman, R.; Lunsford, J. H. *Spectroscopy in Heterogeneous Catalysis*; Academic Press: New York, 1979; p 132.
(41) Topsøe, H.; Dumesic, J. A.; Mørup, S. In *Application of Mössbauer Spectroscopy*; Cohen, R. L., Ed.; Academic Press: New York, 1980; Vol. II, p 55.
(42) Niemantsverdriet, J. W. *Spectroscopy in Catalysis*; VCH: Weinheim, 1995; p 111.
(43) Yamaguchi, T.; Nakano, Y.; Tanabe, K. *Bull. Chem. Soc. Jpn.* **1978**, *51*, 3482.
(44) Nakamoto, K. *Infrared Spectra of Inorganic and Coordination Compounds*; Wiley: New York, 1970; p 98.
(45) Murad, E.; Johnston, J. H. *Mössbauer Spectroscopy Applied to Inorganic Chemistry*; Long, G. J., Ed.; Plenum Press: New York, Vol. 2, p 507.
(46) Ying, Y.; Li, Z.; Hu, J. *Sci. China, Ser. B* **1982**, *25*, 989.
(47) Kündig, W.; Bömmel, H.; Constabaris, G.; Lindquist, R. H. *Phys. Rev.* **1966**, *142*, 327.
(48) Collins, J. F.; Ferguson, I. F. *J. Chem. Soc. A* **1968**, 4.
(49) van der Kraan, A. M. Ph.D. Thesis, Delft University of Technology, 1972.